

**PSFC/JA-12-2**

**First Measurements of Rayleigh-Taylor-Induced  
Magnetic Fields in Laser-produced Plasmas**

*M. J.-E. Manuel, C. K. Li, F. H. Seguin, J. Frenje,  
D. T. Casey, and R. D. Petrasso*

Plasma Science and Fusion Center, Massachusetts Institute of Technology,  
Cambridge, MA

*S. X. Hu, R. Betti, J. Hager, D. D. Meyerhofer, and V. Smalyuk*

Laboratory for Laser Energetics, University of Rochester,  
Rochester, NY

March 2012

**Plasma Science and Fusion Center  
Massachusetts Institute of Technology  
Cambridge MA 02139 USA**

The work described here was done as part of the first author's PhD thesis and supported in part by NLUF/DOE (Grant No. DE-FG03-03SF22691), FSC/DOE (Grant No. DE-FC02-04ER54789), LLE (No. 412160-001G), LLNL (No. B504974), and GA under DOE (DE-AC52-06NA27279).. Reproduction, translation, publication, use and disposal, in whole or in part, by or for the United States government is permitted.

# First Measurements of Rayleigh-Taylor-Induced Magnetic Fields in Laser-produced Plasmas

M. J.-E. Manuel, C. K. Li, F. H. Séguin, J. Frenje, D. T. Casey, and R. D. Petrasso  
*Massachusetts Institute of Technology, Cambridge, MA*

S. X. Hu, R. Betti,\* J. Hager,† D. D. Meyerhofer,\* and V. Smalyuk‡  
*Laboratory for Laser Energetics, University of Rochester, Rochester, NY*  
 (Dated: February 9, 2012)

Experiments with laser-irradiated plastic foils have been performed to investigate Rayleigh-Taylor-induced magnetic and electric fields using a monoenergetic proton radiography system. The first path-integrated B-field strength measurements were inferred from proton radiographs and found to increase from 10 to 100 Tesla- $\mu\text{m}$  during the linear growth phase. Proton fluence modulations were corrected for Coulomb scattering using measured density modulations from X ray radiographs. Under these experimental conditions, estimates of RT-induced B fields indicate Hall parameters of  $\sim 10^{-2}$  for  $\lambda \approx 120 \mu\text{m}$  implying a negligible inhibition of electron transport.

A hydrodynamic system in which the density gradient opposes the acceleration ( $g$ ) is susceptible to the Rayleigh-Taylor [1, 2] (RT) instability. In laser-matter interactions, as seen in inertial confinement fusion (ICF), a continuous density profile is created whereby the ablating mass accelerates into the lighter, expanding plasma, forming an RT-unstable region [3] at the ablation front. During the linear growth phase in a planar geometry small amplitude perturbations, of wavelength  $\lambda$  and amplitude  $a$  on the ablation surface, grow exponentially ( $a = a_0 e^{\gamma t}$ ) until the nonlinearity threshold of  $a \approx \lambda/10$  is reached; during nonlinear growth [4], multimode turbulent effects become important. The RT growth rate of mass perturbations in laser-irradiated targets has been predicted [5, 6], and verified [7, 8] using x-ray based diagnostics, that are insensitive to E and B fields.

During the ablation process, dynamic charge separation and subsequent current generation will create electromagnetic fields [9–11] within the plasma. Ignoring electron inertia, the equations governing self-generated B and E fields can be written as

$$\frac{\partial \mathbf{B}}{\partial t} \approx \nabla \times \left( \frac{\nabla p_e}{en_e} \right) + \nabla \times (\mathbf{v} \times \mathbf{B}), \quad (1)$$

$$\mathbf{E} \approx -\frac{\nabla p_e}{en_e} - \mathbf{v} \times \mathbf{B}. \quad (2)$$

The curl of the isotropic pressure gradient is the primary source of magnetic field generation in Equation 1. This is the familiar [10] thermo-electric (or Biermann battery) term, driven by non-collinear temperature and density gradients. A Fourier analysis of the linearized equations by Nishiguchi [12] showed that RT-induced magnetic fields are  $\pi/2$  out of phase with density modulations during linear growth. B-field generation and evolution are complex processes and a simple linear model is not sufficient to accurately describe the dynamics.

Numerical simulations were performed by Mima *et al.* [13] and Nishiguchi *et al.* [12] to estimate the strength of Rayleigh-Taylor-induced magnetic fields in

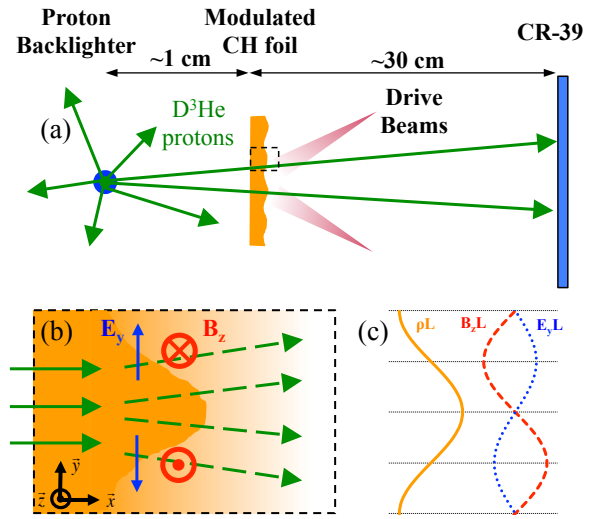


FIG. 1. (a) A schematic drawing of the experimental setup used to radiograph directly-driven plastic (CH) foils with 2D seed perturbations. Proton images are recorded on CR-39 nuclear track detectors. In x ray radiography experiments, a uranium foil backlighter was used, and images taken on film. (b) An expanded view of proton (green) deflections due to RT-induced density, E field (blue), and B field (red) modulations in the target. (c) Path-integrated quantities (arbitrary units) are shown during the linear growth phase.

laser-ablated targets. Acceleration of ablated material generates an RT-unstable region, perturbations will grow and induce magnetic fields. Although the calculations in [12, 13] were performed under different initial conditions, both predicted  $|B_{\text{max}}| \sim 10\text{--}100 \text{ T}$ . Fields of this magnitude near the ablation front of laser-driven ICF capsules may affect electron thermal conduction and inhibit effective ablative drive. The Hall Parameter,  $\chi = \omega \tau \propto B T_e^{3/2} / n_i$ , provides a metric for the decrease in thermal conduction [11] due to B fields. The simulations [12, 13] indicated a Hall parameter of order  $\chi \sim 1$  that

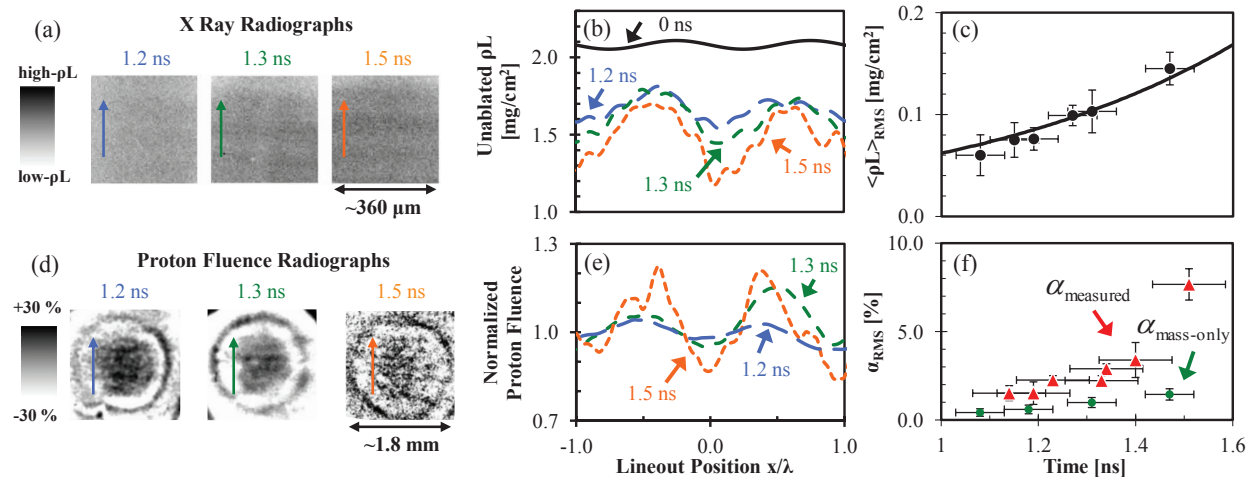


FIG. 2. (a) Sample x-ray radiographs at three times relative to the 2 ns laser drive; scale size is given in the target plane and the lineout direction is indicated. (b) Inferred areal density lineouts from the radiographs shown in a). The nominal value for 0 ns is also shown for comparison. (c) Measured RMS areal densities ( $\bullet$ ) from x-ray radiographs and predicted values (solid) from DRACO. (d) Sample proton fluence radiographs at similar times as x ray images in a); scale size is given in the target plane and lineout direction is indicated. (e) Corresponding lineouts for radiographs in d) are normalized for comparison across different shots. (f) Measured RMS fluence variations ( $\blacktriangle$ ) in proton radiographs. Expected RMS variation due to mass only ( $\bullet$ ) was calculated using density distributions from x-ray data.

will reduce the electron thermal conduction by  $\sim 50\%$  in laser driven ICF. This letter provides the first experimental observations of RT-induced magnetic fields. A novel method for quantifying these fields in planar targets was developed using a combination of proton and x ray radiography.

Experiments were performed on the OMEGA laser [14] using the setup shown in Figure 1a. CH foils,  $21 \pm 2$   $\mu\text{m}$  thick, were seeded with 2D sinusoidal perturbations of wavelength  $\lambda = 120 \pm 2$   $\mu\text{m}$  and amplitude  $a_0 = 0.27 \pm 0.02$   $\mu\text{m}$ . Twelve OMEGA beams were overlapped to directly drive modulated foils over a 2 ns square pulse providing an intensity of  $\sim 4 \times 10^{14}$   $\text{W}/\text{cm}^2$  in a  $\sim 800$   $\mu\text{m}$  diameter spot. To provide uniform illumination across the target, beams were smoothed by spectral dispersion [15] (SSD), SG4 distributed phase plates [16] (DPPs), and distributed polarization rotators [17] (DPRs). In proton backlighting experiments,  $\text{D}^3\text{He}$  protons are deflected in the target by field and mass modulations as shown in Figure 1b. The strength of path-integrated mass and fields, as illustrated in Figure 1c, determines the amount of proton deflection. X ray experiments were performed to quantify mass modulations under these target and laser conditions.

X ray radiographs provided measurements of density-modulation growth in the target. Face-on images were obtained using  $\sim 1.3$  keV x rays from a uranium back-lighter and a streak camera [8, 18] having a temporal resolution of  $\sim 80$  ps and a spatial resolution of  $\sim 10$   $\mu\text{m}$ . Sample x ray radiographs [19] are shown in Figure 2a with the corresponding unablated  $\rho L$  lineouts illustrated in Figure 2b. The decrease in mean  $\rho L$  shown

in Figure 2b is consistent with a mass ablation rate of  $\dot{m} \approx 4 \times 10^5$   $\text{g}/\text{cm}^2/\text{s}$ . The RMS areal densities are calculated and plotted in Figure 2c. For comparison, the 2D code DRACO [20] simulated the radiative hydrodynamics of the RT growth in these experiments using measured foil parameters and a constant flux limiter of 0.06. Predicted density modulations were benchmarked with x ray radiographs as shown by the solid line in Figure 2c. An exponential fit to RMS areal density measurements, independent of simulations, indicate linear growth up to  $t \sim 1.5$  ns with a growth rate of  $\gamma \approx 2.2$   $\text{ns}^{-1}$ .

Monoenergetic proton radiography [21, 22] was used to probe RT-induced electromagnetic field structures. A thin-glass, exploding pusher filled with  $\text{D}^3\text{He}$  gas is imploded by 20 laser beams on the OMEGA laser. Monoenergetic fusion protons (15 MeV) are produced and broadened (3%) by thermal effects and by time-varying E fields around the implosion capsule when nuclear production occurs during the laser pulse. [23] This backlighting technique provides a quasi-isotropic, monoenergetic proton source with an approximately Gaussian emission profile with  $\text{FWHM} \sim 45$   $\mu\text{m}$  and burn duration of  $\sim 150$  ps, as demonstrated [24–27] in many experiments. The proton fluence image is recorded on 10 cm  $\times$  10 cm sheets of CR-39.

The total amplitude modulation observed in proton fluence is due to a combination of perturbing effects from both field deflections and Coulomb scattering,  $\alpha_{RMS}^2 = \alpha_{B/E}^2 + \alpha_{mass}^2$ . The Coulomb scattering component is assessed from the x-ray inferred density modulations and shown to be small. The amount of deflection undergone by a proton caused by B or E fields is proportional

to the path-integrated field strength;  $\theta_B \propto \int B_{\perp} dl$ ,  $\theta_E \propto \int E_{\perp} dl$ , where  $\perp$  indicates the component perpendicular to the proton trajectory. As a result, information regarding path-integrated field strength is encoded within proton fluence modulations. RT-induced modulations in the plasma cause local broadening of the proton fluence due to Coulomb scattering and the Lorentz force, as illustrated in Figure 1b. Fluence perturbations in the center of proton radiographs are primarily due to field structures at the fundamental frequency of the perturbation wavelength.

Proton radiographs of modulated foils were taken over the course of three different shot days, providing data at different times during plasma evolution. Figure 2d shows sample proton fluence radiographs[28] corresponding to similar times as sample x ray radiographs shown in Figure 2a. Proton fluence lineouts from radiographs are normalized for comparison across different experiments and shown in Figure 2e. During the times sampled, coherent linear features are observed and proton fluence variation is calculated from individual lineouts of each radiograph.

A Discrete Fourier Transform (DFT) and resultant power spectrum[29] of each lineout is used to extract the power density at the known perturbation wavelength. The normalized RMS amplitude modulation is defined as  $\alpha_{RMS} \equiv \sqrt{P_f/P_0}$ , where  $P_f$ [30] is the power density at the fundamental frequency of interest and  $P_0$  is the power at zero frequency (for normalization). This corresponds to the RMS of a sinusoid with frequency  $f$  normalized to the average. A Wiener Filter removes contributions to  $\alpha_{RMS}$  from non-seed-perturbation effects, such as surface roughness of the foil and residual laser imprint. [18] Resulting  $\alpha_{RMS}$  values are shown ( $\blacktriangle$ ) in Figure 2f and are shown to increase up to  $t \sim 1.5$  ns. Expected proton fluence modulations due to measured density distributions were calculated using the Monte Carlo code[31] Geant4 [32] and shown ( $\bullet$ ) in Figure 2f to be 3–5 times less than measured proton modulations.

The mass contribution to  $\alpha_{RMS}$  is removed, and the residual is attributed to deflections due to RT-induced magnetic and/or electric fields,  $\alpha_{B/E} = \sqrt{\alpha_{RMS}^2 - \alpha_{mass}^2}$ . Assuming a sinusoidally varying field during linear growth, as in the Nishiguchi model[12], expected  $\alpha_{B/E}$  values were mapped to path-integrated field values. [33] RMS magnetic fields ( $\langle BL \rangle_{RMS}$ ) or electric fields ( $\langle EL \rangle_{RMS}$ ) are inferred from proton fluence modulation measurements by attributing residual amplitude modulations to *only magnetic fields* (Figure 3a) or *only electric fields* (Figure 3b). To determine whether B or E dominates proton deflection at the target, a simple model for estimating field strengths was implemented.

Magnetic and electric field evolution are described in the ideal MHD limit by Equations 1 and 2. Because magnetic Reynolds numbers are large ( $Re_m \sim 100-1000$ ) [34] during laser illumination, magnetic diffusion may be neglected and an ideal MHD treatment is sufficient, though

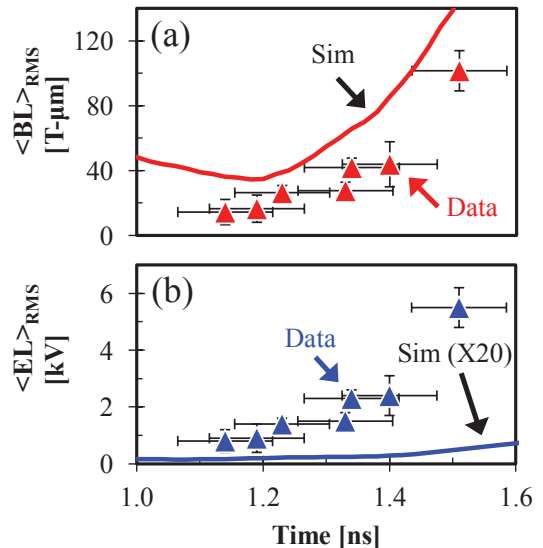


FIG. 3. Inferred path-integrated quantities ( $\blacktriangle$ ) are calculated from measured  $\alpha_{RMS}$  values if deflections are caused by (a) B-fields and mass, or (b) E-fields and mass. Simulated B fields indicate an approximate upper estimate and are a factor of  $\sim 2$  higher than inferred values, whereas simulated E fields are a factor of  $\sim 100$  too low to account for measured proton fluence modulations.

represents an approximate upper estimate [35] of B field strength. In this limit, B field evolution is described by Equation 1 and is analogous to the fluid vorticity equation. Therefore, the B field is found to be proportional to the fluid vorticity. Using the hydrodynamic predictions from DRACO, B field distributions were computed by [35]

$$\mathbf{B} \approx \frac{m_p A}{e(Z+1)} \nabla \times \mathbf{v}, \quad (3)$$

where  $m_i$  is the ion mass and  $Z$  the charge state. E fields were then calculated by Equation 2 using the electron pressure and number density distributions from DRACO in conjunction with computed B fields. Simulated B and E fields were integrated in the direction of proton propagation up to the critical surface and RMS path-integrated field values were calculated for comparison with measured proton data. The RMS path-integrated B and E field estimates are shown by solid lines in Figure 3. Predicted  $\langle BL \rangle_{RMS}$  values were found to be higher than measurements by a factor of  $\sim 2$ , but predicted  $\langle EL \rangle_{RMS}$  values were found to be low by a factor of  $\sim 100$ . It should be noted that these calculations do not include Nernst convection [36],  $\mathbf{v}_N \propto -\tau_{ei} \nabla T$  which may enhance the magnetic field strength. Despite simplifications in this model, path-integrated field estimates clearly indicate that proton deflections are dominantly due to magnetic fields, not electric fields.

Magnetic field magnitudes were estimated from path-

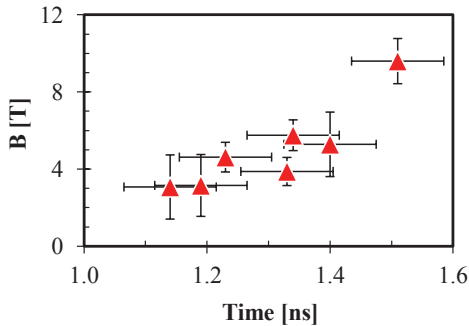


FIG. 4. B field amplitudes inferred from path-integrated measurements. The scale length of the field structure in the direction of proton propagation is approximated as the peak-to-valley amplitude of the perturbation at each sample time.

integrated measurements by using the peak-to-valley perturbation amplitude ( $h = 2a$ ) as a scale size for field structure. The initial perturbation amplitude  $a_0 = 0.27 \mu\text{m}$  grows exponentially as  $a = a_0 e^{\gamma t}$  where, from x ray measurements,  $\gamma \approx 2.2 \text{ ns}^{-1}$ . Magnetic field amplitudes are computed as  $B \approx \sqrt{2} \langle BL \rangle_{\text{RMS}} / h$  and shown in Figure 4 (the factor  $\sqrt{2}$  relates RMS to peak amplitude for sinusoidal functions). Resultant B field amplitude estimates increase from  $\sim 3$  to  $\sim 9$  T during the linear growth phase. In these directly driven experiments, electron temperatures and densities near the ablation surface are estimated from simulations to be a few hundred eV and a few  $\sim 10^{22} \text{ cm}^{-3}$ , respectively. Under these conditions, the magnetic fields caused by  $\lambda \approx 120 \mu\text{m}$  perturbations result in a Hall parameter of  $\chi \sim 10^{-2}$ , indicating a minimal effect ( $< 1\%$ ) on electron thermal conduction.

In summary, the first measurements of RT-induced magnetic fields in laser-produced plasmas is reported. X ray radiographs were used to measure density modulations in laser-irradiated  $21 \mu\text{m}$  thick CH targets with imposed sinusoidal perturbations of wavelength  $\lambda \approx 120 \mu\text{m}$  and initial amplitudes of  $a_0 \approx 0.27 \mu\text{m}$ . Using monoenergetic proton radiography, images were taken of foils at select times during the linear phase of RT growth. It was shown that proton deflections due to RT-induced field structures are dominated by magnetic, not electric, fields. After compensating for proton scattering due to measured density modulations, path-integrated B fields were inferred from proton fluence radiographs and found to increase from  $\sim 10$  to  $\sim 100 \text{ T}\cdot\mu\text{m}$ , corresponding to a Hall parameter of order  $\chi \sim 10^{-2}$ . Observations made herein motivate further investigation into RT-induced field structures at later times and under different conditions using proton radiography. Furthermore, measured B field strengths imply, at least for  $\lambda \approx 120 \mu\text{m}$  and these laser conditions, negligible inhibition of electron thermal transport in direct-drive ICF.

The authors express their gratitude to the engineering staff at LLE for their support. The work described here was done as part of the first author's PhD thesis and supported in part by NLUF/DOE (Grant No. DE-FG03-03SF22691), FSC/DOE (Grant No. DE-FC02-04ER54789), LLE (No. 412160-001G), LLNL (No. B504974), and GA under DOE (DE-AC52-06NA27279).

- 
- \* also at the Dept. of Mechanical Engineering and Physics  
 † now at State University of New York, Geneseo  
 ‡ now at Lawrence Livermore National Laboratories
- [1] J. W. Strutt. Proc London Math Soc, **14**, 8 (1883).
  - [2] G. Taylor. Proc Roy Soc of London, **201**, 192 (1950).
  - [3] J. D. Lindl, et al. Phys Plasma, **11**, 339 (2004).
  - [4] S. W. Haan. Phys Rev A, **39**, 5812 (1989).
  - [5] H. Takabe, et al. Phys Fluid, **28**, 3676 (1985).
  - [6] R. Betti, et al. Phys Plasma, **5**, 1446 (1998).
  - [7] B. A. Remington, et al. Phys Rev Lett, **73**, 545 (1994).
  - [8] V. A. Smalyuk, et al. Phys Plasma, **15**, 082703 (2008).
  - [9] J. A. Stamper, et al. Phys Rev Lett, **26**, 1012 (1971).
  - [10] M. G. Haines. Can J Phys, **64**, 912 (1986).
  - [11] S. I. Braginskii. *Transport processes in a plasma*, volume 1 of *Reviews of Plasma Physics*. Consultants Bureau, New York (1965).
  - [12] A. Nishiguchi. Japan J App Phys, **41**, 326 (2002).
  - [13] K. Mima, et al. Phys Rev Lett, **41**, 1715 (1978).
  - [14] T. R. Boehly, et al. Opt Comm, **133**, 495 (1997).
  - [15] S. P. Regan, et al. J. Opt. Soc. Am. B, **17**, 1483 (2000).
  - [16] Y. Lin, et al. Opt. Lett., **20**, 764 (1995).
  - [17] T. R. Boehly, et al. Journal of Applied Physics, **85**, 3444 (1999).
  - [18] V. A. Smalyuk, et al. Rev Sci Inst, **70**, 647 (1999).
  - [19] X ray data shown from OMEGA shot 50870.
  - [20] D. Keller, et al. *DRACO—A New Multidimensional Hydrocode* (1999).
  - [21] C. K. Li, et al. Phys Plasma, **16**, 056304 (2009).
  - [22] C. K. Li, et al. Phys Rev Lett, **97**, 135003 (2006).
  - [23] C. K. Li, et al. Phys Plasma, **7**, 2578 (2000).
  - [24] F. H. Séguin, et al. Physics of Plasmas, **19**, 12 (2012).
  - [25] J. R. Rygg, et al. Science, **319**, 1223 (2008).
  - [26] C. K. Li, et al. Phys Rev Lett, **100**, 225001 (2008).
  - [27] R. D. Petrasso, et al. Phys Rev Lett, **103**, 085001 (2009).
  - [28] Proton radiographs from OMEGA shots 49109 (1.2 ns), 61721(1.3 ns), 49111(1.5 ns).
  - [29] W. H. Press, et al. *Numerical Recipes in C++: The Art of Scientific Computing Second Edition*. Cambridge University Press, 2 edition (2002).
  - [30] Power density is calculated from the DFT as  $P_f = |c_f|^2/2$  where  $c_f$  is the complex Fourier coefficient at frequency  $f$  using a Hann windowing function.
  - [31] Geant4 uses a cold-matter approximation.
  - [32] J. Allison, et al. IEEE Trans Nuc Sci, **53**, 270 (2006).
  - [33] M. J.-E. Manuel, et al. Phys Plasma, **to be sub.** (2012).
  - [34] C. K. Li, et al. Physical Review Letters, **99**, 055001 (2007). Copyright (C) 2010 The American Physical Society Please report any problems to prola@aps.org PRL.
  - [35] R. G. Evans. Plasma Phys Cont Fus, **28**, 1021 (1986).
  - [36] A. Nishiguchi, et al. Phys Rev Lett, **53**, 262 (1984).